RAPID COMMUNICATION | NOVEMBER 27 2024

Revisiting the Green–Kubo relation for friction in nanofluidics

Anna T. Bui ; Stephen J. Cox

J. Chem. Phys. 161, 201102 (2024)
https://doi.org/10.1063/5.0238363

The Journal of Chemical Physics COMMUNICATION pubs.aip.org/aip/jcp

Revisiting the Green–Kubo relation for friction in nanofluidics

Cite as: J. Chem. Phys. 161, 201102 (2024); doi: 10.1063/5.0238363
Submitted: 11 September 2024 • Accepted: 12 November 2024 •
Published Online: 27 November 2024

Anna T. Bui[1] and Stephen J. Cox[1,2,a)]

AFFILIATIONS

[1] Yusuf Hamied Department of Chemistry, University of Cambridge, Lensfield Road, Cambridge CB2 1EW, United Kingdom
[2] Department of Chemistry, Durham University, South Road, Durham DH1 3LE, United Kingdom

[a)] Author to whom correspondence should be addressed: stephen.j.cox@durham.ac.uk

ABSTRACT

A central aim of statistical mechanics is to establish connections between a system's microscopic fluctuations and its macroscopic response to a perturbation. For non-equilibrium transport properties, this amounts to establishing Green–Kubo (GK) relationships. In hydrodynamics, relating such GK expressions for liquid–solid friction to macroscopic slip boundary conditions has remained a long-standing problem due to two challenges: (i) The GK running integral of the force autocorrelation function decays to zero rather than reaching a well-defined plateau value, and (ii) debates persist on whether such a transport coefficient measures an intrinsic interfacial friction or an effective friction in the system. Inspired by ideas from the coarse-graining community, we derive a GK relation for liquid–solid friction where the force autocorrelation is sampled with a constraint of momentum conservation in the liquid. Our expression does not suffer from the "plateau problem" and unambiguously measures an effective friction coefficient, in an analogous manner to Stokes' law. We further establish a link between the derived friction coefficient and the hydrodynamic slip length, enabling a straightforward assessment of continuum hydrodynamics across length scales. We find that continuum hydrodynamics describes the simulation results quantitatively for confinement length scales all the way down to 1 nm. Our approach amounts to a straightforward modification to the present standard method of quantifying interfacial friction from molecular simulations, making possible a sensible comparison between surfaces of vastly different slippage.

I. INTRODUCTION

Describing the flow of liquids at solid surfaces is essential for understanding many physical processes of both fundamental and technological importance, including transport through membranes and nanopores, power generation, desalination, and electrokinetic effects.[1–3] Unlike in the bulk, fluid transport under confinement is governed by frictional forces arising from momentum transfer at the liquid–solid interface. Over the past decade, advances in device fabrication[4–6] have spurred increased interest in nano-confined water, with many experimental and simulation studies reporting exotic friction effects in "one-dimensional" (1D) nanotubes and "two-dimensional" (2D) nanochannels.[7–21] A natural consequence of confinement is that as the confining volume is decreased, the surface-to-volume ratio increases, which amplifies the impact of interfacial effects on transport properties, such as friction. In addition to dissipation processes at the interface, viscous effects in the liquid itself also contribute to the effective friction in the system. Therefore, it is essential to distinguish these competing effects by quantifying an intrinsic surface property that is independent of the confining volume.

From a macroscopic perspective, such a property is the slip length b, measuring the distance beyond the surface of the wall at which the fluid velocity $v_x(z)$ extrapolates to zero. The slip length enters a continuum hydrodynamics description, hereafter referred to as "classical hydrodynamic theory" (CHT), as a boundary condition to the Navier–Stokes equations,

$$\left.\frac{\partial v_x}{\partial z}\right|_{z=z_0} = \frac{v_s}{b}, \tag{1}$$

relating the velocity gradient to the slip velocity $v_s = v_x(z_0)$. The $z = z_0$ plane is where the hydrodynamic boundary position is placed. The no-slip boundary condition $b = 0$ applies for surfaces that are highly sticky, while for atomically smooth and non-wetting surfaces where there is finite slippage at the interface, $b > 0$. The gradient of

the fluid velocity is linearly related to the viscous stress of the fluid $\sigma_{xz} = -\eta(\partial v_x/\partial z)$, where η is the shear viscosity (which we assume takes its bulk value in all regions occupied by the fluid). The stress is itself balanced by the friction force from the solid to the liquid F_x per unit surface area $\mathcal{A}$. This allows a linear relation between F_x and v_s to be written,

$$F_x = -\lambda_{\text{intr}}\,\mathcal{A} v_s. \tag{2}$$

Equation (2) is known as Navier's interfacial constitutive relation,[22] defining an intrinsic friction coefficient λ_{intr}. Both λ_{intr} and b are intrinsic properties of the interface and are related by

$$\lambda_{\text{intr}} = \frac{\eta}{b}. \tag{3}$$

It has been established that in the linear response regime, b (and therefore λ_{intr}) is independent of both the type of flow (i.e., Couette or Poiseuille) and the channel height,[23] provided that the length scale of confinement is large enough for CHT to faithfully describe hydrodynamic transport. Quantifying "large enough" is something that the framework we present in this Communication allows us to directly assess with molecular simulations; generally speaking, we find CHT works with as few as two or three layers of water.

In experiments,[7–10,12] to measure transport coefficients, such as λ_{intr}, one would drive the system of interest out of equilibrium and measure the responding flux to the driving force. The resulting force–flux relation obtained can then be mapped back onto predictions from CHT, and b or λ_{intr} can be backed out accordingly. While an analogous strategy can, in principle, be followed in molecular simulations, methods using non-equilibrium molecular dynamics (NEMD) are limited by statistical sampling and delicate issues that arise in thermostatting the system.[24]

From a microscopic perspective, frictional effects coming from dissipation in the liquid manifest through balance of forces at non-equilibrium steady states. A natural question to ask is if one can relate these transport coefficients to equilibrium fluctuations in the liquid, invoking Onsager's regression hypothesis. In this context, one attempts to seek Green–Kubo (GK) expressions for a liquid–solid friction coefficient, allowing the hydrodynamic boundary conditions to be characterized from a single equilibrium molecular dynamics (EMD) simulation. The seminal work by Bocquet and Barrat[25,26] (BB) proposed such a relation for λ_{intr}, given as

$$\lambda_{\text{BB}} = \frac{\beta}{\mathcal{A}}\int_0^\infty \mathrm{d}t\,\langle F_x(t)F_x(0)\rangle, \tag{4}$$

where $\beta = 1/(k_B T)$, k_B is the Boltzmann constant, T is temperature, and $\langle\ldots\rangle$ indicates an ensemble average at equilibrium. Such a GK relation involving the force autocorrelation function is similar to the expression for friction ξ of a heavy Brownian particle immersed in a bath of lighter particles, as derived from Langevin dynamics. In Ref. 26, BB presented a derivation for Eq. (4) from a Langevin equation for the stochastic motion of the solid wall immersed in the fluid.

However, two major challenges arise upon application of Eq. (4) to measure friction at the liquid–solid interface. The first issue is the well-documented "plateau problem,"[27–34] referring to the fact that the integral in Eq. (4) in general will decay to zero at long time. While this behavior is often attributed to the swapping of the order in which the thermodynamic and long-time limits are taken,[26,29,30,33,35] we will show—as becomes clear when employing a Mori–Zwanzig formalism to derive the appropriate Langevin dynamics—that this is in fact a direct consequence of using real forces rather than projected forces in Eq. (4). The plateau problem is most severe when the surface is strongly wetting or when the liquid film is very thin (see Fig. S2 of the supplementary material).

The second major challenge involves the intense debate whether λ_{BB} provides a measure of the intrinsic friction coefficient λ_{intr} or the effective friction of the entire system.[35–41] From the perspective of Langevin theory, the friction coefficient ξ characterizes the total dissipation associated with the motion of the Brownian particle through the solvent, rather than just the intrinsic slippage at the particle's surface. Therefore, directly relating Eq. (4) to the intrinsic friction λ_{intr} is not straightforward. These issues have thus made it difficult to faithfully assess friction under confinement across different length scales using Eq. (4). In this context, we note the work of Petravic and Harrowell, who pointed out that for Couette flow, the friction measured by λ_{BB} includes contributions both from the slip at the interface and from viscous dissipation in the fluid.[36] Nonetheless, the GK relation given by Eq. (4) continues to be widely applied in the community.[16,17,20,42–47] However, its use is often limited to surfaces of high slippage. There is thus a significant need to establish both a practical solution to the plateau problem and a rigorous connection between the GK transport coefficient and the intrinsic friction defined by CHT.

In this Communication, we present a derivation of a GK relation for liquid–solid friction by considering the liquid's stochastic motion in the solid's frame of reference, using the Mori–Zwanzig projection operator formalism and linear response theory. The resulting expression for the friction coefficient, which overcomes the plateau problem, involves sampling the force autocorrelation function with a simple momentum conservation constraint on the liquid. We also show that this friction coefficient measures an effective friction of the system rather than the intrinsic friction. By making an appropriate mapping to CHT, we then nonetheless relate λ_{eff} directly to the hydrodynamic slip length b. We use the resulting framework to faithfully assess interfacial friction arising from water flow in 1D tubes and 2D channels across a wide range of confining length scales, including results from first-principles-level simulations.

II. THE GREEN–KUBO RELATION FOR FRICTION

A. Mori–Zwanzig projection operator formalism

At the heart of any friction problem is a separation of timescales for different degrees of freedom. In the textbook problem of Brownian motion, the two timescales at play are evident: one associated with the slow motion of the heavy Brownian particle and one with its frequent collisions with lighter solvent particles, which constitute "the bath." Instead of describing the complex system as a whole, one tends to focus only on the motion of the Brownian particle as a coarse-grained variable, with the rapid collisions with the solvent treated as a fluctuating random force. This approach underpins the Langevin equation, which describes the Brownian particle's motion using a combination of a frictional drag force and a fluctuating random force. More generally, this description can also be

applied to an arbitrary coarse-grained variable in any complex system, provided that the variable evolves on a slower timescale than the rest of the system. This is an important result of Mori–Zwanzig theory,[48,49] where projection operators are used to derive generalized Langevin equations for coarse-grained variables. Detailed presentation of Mori–Zwanzig theory can be found in standard texts,[50–52] and here we will review only the most salient aspects for the job at hand.

For any phase variable A evolving under equations of motion from a specified Hamiltonian $\mathcal{H}$, its time evolution obeys the Liouville equation,

$$\frac{\mathrm{d}A(t)}{\mathrm{d}t} = i\mathcal{L}A(t), \tag{5}$$

which has the formal solution $A(t) = \mathrm{e}^{i\mathcal{L}t}A(0)$, where $i\mathcal{L}$ denotes the Liouville operator associated with $\mathcal{H}$. For any observable B, we can denote its projection onto A with a projection operator $\mathcal{P}$,

$$\mathcal{P}B(t) = (B(t), A)(A, A)^{-1}A, \tag{6}$$

where $(\cdots, \cdots)$ denotes a scalar product,

$$(B(t), A) = \int \mathrm{d}\Gamma\, f_0(\Gamma)B(\Gamma, t)A^*(\Gamma), \tag{7}$$

with $f_0(\Gamma)$ the equilibrium distribution of initial phase space points Γ. The complementary operator $\mathcal{Q} = \mathbb{1} - \mathbb{P}$ projects onto the subspace orthogonal to A such that

$$(\mathcal{Q}B(t), A) = 0. \tag{8}$$

The time evolution of the stochastic coarse-grained variable A is given by the generalized Langevin equation,

$$\frac{\mathrm{d}A(t)}{\mathrm{d}t} = i\Omega A(t) - \int_0^t \mathrm{d}t'\, K(t - t')A(t') + F^{\mathrm{R}}(t), \tag{9}$$

where $i\Omega$ ("the frequency"), K ("the memory function"), and F^{R} ("the random force") are well-defined functions. When A is a single coarse-grained variable, $i\Omega = 0$. The memory function is related to the autocorrelation of the random force,

$$K(t) = (F^{\mathrm{R}}(t), F^{\mathrm{R}})(A, A)^{-1}, \tag{10}$$

while the random force itself is given by the projection of $\dot{A}$ orthogonal to A,

$$F^{\mathrm{R}}(t) = \mathrm{e}^{i\mathcal{Q}\mathcal{L}t}F^{\mathrm{R}}(0), \tag{11}$$

where $F^{\mathrm{R}}(0) = \mathcal{Q}\dot{A}(0)$. An important consequence of the orthogonal projection in the random force is the lack of correlation between F^{R} and A, i.e.,

$$(F^{\mathrm{R}}(t), A) = 0, \tag{12}$$

which is at the foundation of the Onsager regression hypothesis.

When A relaxes much more slowly than the random noise, which implicitly assumes that it is the only slow degree of freedom, the memory function can be treated in the Markovian approximation: $K(t) = 2\Lambda\delta(t)$. The generalized Langevin equation [Eq. (9)] then simplifies to the Langevin equation,

$$\frac{\mathrm{d}A(t)}{\mathrm{d}t} = -\Lambda A(t) + F^{\mathrm{R}}(t), \tag{13}$$

where a time-independent friction coefficient is given as

$$\Lambda = \int_0^\infty \mathrm{d}t\, (\mathrm{e}^{i\mathcal{Q}\mathcal{L}t}F^{\mathrm{R}}, F^{\mathrm{R}})(A, A)^{-1}. \tag{14}$$

B. Applying the operator formalism to liquid–solid friction

To describe liquid–solid friction, we will consider the problem of a liquid droplet's stochastic motion on a solid surface, schematically shown in Fig. 1(a). We choose this arrangement both for conceptual simplicity and to make the connection between this derivation and that for Brownian motion clear; the resulting framework, however, is readily applied to systems comprising a fluid confined between walls. We will work in the solid's frame of reference so that we can consider it to be at rest. The liquid droplet comprises N particles, whose positions and momenta are $\{\boldsymbol{r}_i, \boldsymbol{p}_i\}$ and has a total mass of $M = \sum_{i=1}^N m_i$. For simplicity, we will focus only on the droplet's motion in the x direction, with a center-of-mass velocity of $\bar{v}_x$.

Provided that the droplet is sufficiently large, two very different timescales can be identified in this problem: one associated with the slow motion of the droplet undergoing a random walk on the surface and one associated with frequent collisions between individual liquid particles and the solid. Analogous to Brownian motion, we therefore now treat the total linear momentum of the liquid droplet $P_x = M\bar{v}_x$ as the coarse-grained variable of interest. Its time evolution is governed by

$$\frac{\mathrm{d}P_x(t)}{\mathrm{d}t} = i\mathcal{L}P_x(t) \qquad [\text{real dynamics}], \tag{15}$$

for which the solution is $P_x(t) = \mathrm{e}^{i\mathcal{L}t}P_x(0)$, where the Liouville operator is explicitly given as

$$i\mathcal{L} = \sum_{i=1}^N \left(\frac{\boldsymbol{p}_i}{m_i} \cdot \frac{\partial}{\partial \boldsymbol{r}_i} + \boldsymbol{f}_i \cdot \frac{\partial}{\partial \boldsymbol{p}_i} \right), \tag{16}$$

where $\boldsymbol{f}_i$ is the force on each liquid particle. We will refer to the dynamics associated with $i\mathcal{L}$ as the "real dynamics," i.e., those that result from propagating Newton's equations of motion in standard MD simulations. Upon application of the result in Eq. (13), which implies a Markovian approximation, the liquid motion can be described with

$$M\frac{\mathrm{d}\bar{v}_x(t)}{\mathrm{d}t} = -\lambda_{\mathrm{eff}}\mathcal{A}\bar{v}_x(t) + F^{\mathrm{R}}(t), \tag{17}$$

where λ_{eff} is an effective friction coefficient. The term $-\lambda_{\mathrm{eff}}\mathcal{A}\bar{v}_x(t)$ measures the frictional drag force on the liquid droplet as a whole, rather than the intrinsic friction due to slippage at the interface $-\lambda_{\mathrm{intr}}\mathcal{A}\bar{v}_s$ as in Eq. (2) (see Sec. III A). The random force is now

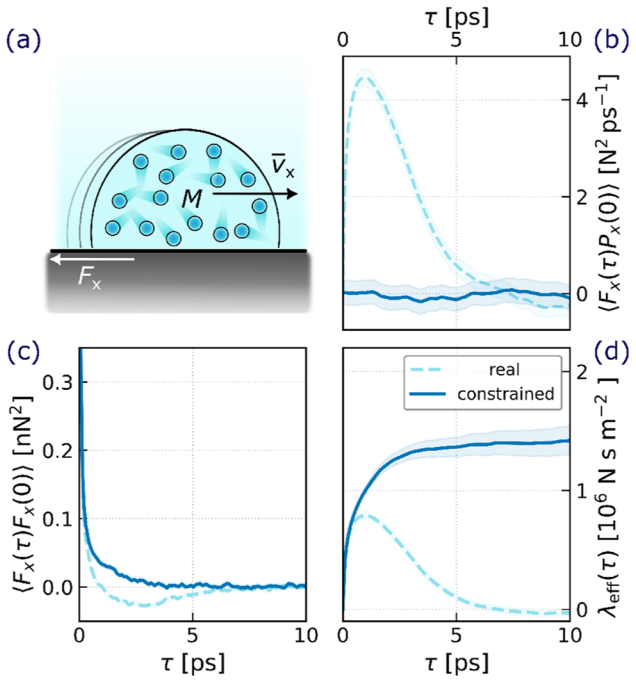

FIG. 1. The Green–Kubo friction integral. (a) Schematic of the system setup that we use for the derivation; a liquid droplet of total mass M moves stochastically on a solid surface. Its center-of-mass velocity along one direction is indicated by $\bar{v}_x$, and the frictional force with the surface is F_x. For a liquid–solid interface with high wettability (see Sec. III B), we show (b) the force–momentum correlation function, (c) the force–force autocorrelation function, and (d) the friction GK integral. Using real dynamics results in a plateau problem since the force is correlated with the momentum, leading to negative correlation in the force autocorrelation; this causes the GK integral to vanish at long times. Constrained dynamics bypasses this issue by imitating the effect of projected forces, ensuring that the integral plateaus to a finite value.

given by the orthogonal projection of total tangential force on the liquid,

$$F^{\mathrm{R}}(t) = \mathrm{e}^{i\mathcal{Q}\mathcal{L}t}F^{\mathrm{R}}(0), \tag{18}$$

where $F^{\mathrm{R}}(0) = \dot{P}_x(0) = F_x(0)$. Using the fluctuation–dissipation theorem as stated in Eq. (14) and the equipartition theorem $M\langle \bar{v}_x^2\rangle = k_{\mathrm{B}}T$, the friction coefficient is given as

$$\lambda_{\mathrm{eff}} = \frac{\beta}{\mathcal{A}}\int_0^\infty \mathrm{d}t\ (\mathrm{e}^{i\mathcal{Q}\mathcal{L}t}F_x, F_x). \tag{19}$$

According to Eq. (19), to obtain λ_{eff}, the force autocorrelation function should be sampled with projected dynamics propagated by $i\mathcal{Q}\mathcal{L}$. However, such a dynamical scheme is not readily realizable in MD simulations, since, in general, it is not possible write the projection operator $\mathcal{Q}$ explicitly. To make progress, a common though ad hoc assumption to make is that the random force evolves with $i\mathcal{L}$ instead of $i\mathcal{Q}\mathcal{L}$, i.e., $F^{\mathrm{R}}(t) \approx \mathrm{e}^{i\mathcal{L}t}F_x(0)$. The BB formula given by Eq. (4) amounts to such an approximation. Although the GK formula in Eq. (4) can be sampled directly in a MD simulation, a consequence of replacing $i\mathcal{Q}\mathcal{L}$ with $i\mathcal{L}$ is that the random force is no longer uncorrelated with the coarse-grained variable P_x, violating the condition stated in Eq. (12). The effect is easily seen in the results of MD simulations. For a water film ~2.7 nm in thickness in contact with a strongly wetting surface (see Sec. III B), we see in Fig. 1(b) that $\langle F_x(\tau)P_x(0)\rangle$ initially shows a large positive correlation, exhibiting a weak negative correlation at longer times. Such a correlation between the force and the momentum leads to a negative contribution to the force autocorrelation function, as shown in Fig. 1(c), making the integral in Eq. (4) vanish at long times, as seen in Fig. 1(d). We can also understand why the plateau problem encountered in the use of the BB formula is most severe for surfaces of strong wettability or when the liquid film is very thin. In these cases, since a large portion of momentum in the liquid can be transferred to the solid, F_x and P_x are strongly correlated in the real dynamics, and Eq. (12) is severely violated. Moreover, the Markovian approximation that relaxation of P_x is much slower than all other degrees of freedom also becomes more severe.

C. Momentum conservation constraint to overcome the plateau problem

In fact, the plateau problem has been discussed in the coarse-graining community, where the issues associated with replacing projected dynamics with real dynamics, along with the limitations of the Markovian approximation, are more widely recognized.[53,54] There have also been developments of algorithms for obtaining projected observables of the GLE directly.[55–57] Here, we adopt the strategy proposed in Ref. 53: instead of modeling the real dynamics directly, where the Markovian approximation is only good in certain limits, we aim to construct a constrained dynamics in which the Markovian approximation is enforced. It then becomes a modeling question of how well the constrained dynamics represents the physical behavior of interest. In the context of liquid–solid friction, we validate our results directly against NEMD simulations.

To make such a Markovian approximation exact, we want to ensure a separation of timescales between the motion of the droplet and the other degrees of freedom. To this end, we introduce a constraint on the system that maintains the droplet's linear momentum to be zero at all times. In this picture, the motion of the droplet as a whole is infinitely slow compared to the individual microscopic processes that each fluid particle undergoes. Since P_x does not evolve in time under the constraint, the Liouville equation is trivially

$$\frac{\mathrm{d}P_x(t)}{\mathrm{d}t} = i\mathcal{L}_{\mathrm{c}}P_x(t) = 0 \qquad [\text{constrained dynamics}] \tag{20}$$

such that $P_x(t) = \mathrm{e}^{i\mathcal{L}_{\mathrm{c}}t}P_x(0) = P_x(0) = 0$. The corresponding Liouville operator to fix the momentum of the liquid can be written as

$$i\mathcal{L}_{\mathrm{c}} = \sum_{i=1}^{N}\left[\left(\frac{\boldsymbol{p}_i}{m_i} - \mu\hat{\boldsymbol{e}}_x\right)\cdot\frac{\partial}{\partial \boldsymbol{r}_i} + \left(\boldsymbol{f}_i - \gamma m_i\hat{\boldsymbol{e}}_x\right)\cdot\frac{\partial}{\partial \boldsymbol{p}_i}\right], \tag{21}$$

where $\hat{\boldsymbol{e}}_x$ denotes the unit vector in the x direction and the Lagrange multipliers are $\mu = P_x/M$ and $\gamma = F_x/M$. Such constrained dynamics can be straightforwardly realized in an MD simulation: at equilibrium, the liquid has zero initial momentum, so the constraint should maintain $P_x = 0$, which amounts to simply subtracting the center-of-mass velocity of the liquid at every time step.

An important consequence of the constrained dynamics is that since the liquid momentum P_x is conserved, all other degrees of freedom of the system become uncorrelated with P_x. In other words, they all lie on the subspace orthogonal to P_x such that the effect of the projection operator $\mathcal{Q}$ is already encapsulated, i.e.,

$$\mathcal{Q}i\mathcal{L}_c = (\mathbb{1} - \mathcal{P})i\mathcal{L}_c = i\mathcal{L}_c. \tag{22}$$

The random force is therefore now exactly the force sampled with constrained dynamics,

$$F^R(t) = e^{i\mathcal{L}_c t}F^R(0), \tag{23}$$

where $F^R(0) = \dot{P}_x(0) = F_x(0)$. As a result, we can justifiably replace $i\mathcal{Q}\mathcal{L}$ with $i\mathcal{L}_c$ in Eq. (19), giving an expression for the friction coefficient,

$$\lambda_{\text{eff}} = \frac{\beta}{\mathcal{A}}\int_0^\infty dt\ (e^{i\mathcal{L}_c t}F_x, F_x) \equiv \frac{\beta}{\mathcal{A}}\int_0^\infty dt\ \langle F_x(t)F_x(0)\rangle_c. \tag{24}$$

In the second line, we have used $\langle \ldots \rangle_c$ to denote a canonical average in the constrained system. The lack of correlation in F_x and P_x under constrained dynamics, seen in Fig. 1(b), means that Eq. (12) is always satisfied and there is no negative contribution to the force autocorrelation function, as seen in Fig. 1(c). Therefore, the integral in Eq. (24) always reaches a well-defined plateau value and does not decay to zero, as seen in Fig. 1(d). We will show in Sec. III A that λ_{eff} measures an effective friction of the entire system and not, in general, the liquid–solid interfacial friction.

Equation (24) is a core result of this Communication, presenting a GK relation for liquid–solid friction where the force autocorrelation function is sampled with a zero momentum constraint on the liquid. We stress that the constraint is proposed as a simple way to ensure that the sampled force obeys the orthogonality condition (Eq. (12)) such that the friction coefficient can be obtained from EMD, without explicitly calculating projected forces. While this constrained ensemble is by no means a "physical" model of the system's dynamics, in addition to numerically verifying its usefulness (see Sec. III), we can provide suggestions as to why it might retain many physical properties relevant for describing liquid–solid friction. First, since the constraint does not change the internal energy of the system, the hydrodynamic boundary and surface roughness[14,58] remain unchanged between real and constrained dynamics, as verified by simulations (see Fig. S3). Second, when the liquid droplet is constrained to remain at rest, its center-of-mass motion becomes "infinitely" slower compared to the fast collisions individual liquid particles undergo. While this effectively accelerates the microscopic noise contributing to the random force, at the microscopic scale, each liquid particle on average experiences the same potential energy surface with the same thermal fluctuations, so the overall dissipation in the system should be largely unaffected, provided that liquid droplet is sufficiently big.

III. INTERPRETING THE FRICTION COEFFICIENT

A. The effective friction coefficient is not an intrinsic property of the interface

The friction coefficient λ_{eff} quantifies the dissipation in the system when there is a net relative motion between the liquid and the solid. When the liquid is pushed out of equilibrium, in general, the velocity of the liquid will not be constant across the cross section perpendicular to the direction of the flow. Therefore, in addition to dissipation coming from collisions of liquid particles with the solid at the interface, there are also contributions from viscous forces arising between adjacent layers of the fluid flowing at different velocities away from the interface. This means that λ_{eff} will depend on the amount of liquid present and is not an intrinsic surface property. In fact, the effective friction will only be equal to the intrinsic friction $\lambda_{\text{eff}} \approx \lambda_{\text{intr}}$ either in the limit of a very thin film of liquid or when there is perfect slip ($b = \infty$) at the interface and the velocity profile becomes plug-like; in such cases, the slip velocity is well approximated by the average fluid velocity, $\bar{v}_x \approx v_s$. In this limit, Eq. (17) becomes

$$M\frac{d\bar{v}_x(t)}{dt} = -\lambda_{\text{intr}}\mathcal{A}v_s(t) + F^R(t). \tag{25}$$

At this point, it is instructive to point out the difference in our derivation compared to that of BB in Ref. 26. So far, we have worked in the solid's frame of reference and treated the liquid's motion as the coarse-grained variable. We have then applied the Langevin equation under the Markovian approximation and taken the limit where the velocity profile in the fluid is a constant (plug flow) to arrive at Eq. (25). Meanwhile, BB started out by considering the solid wall's motion as the coarse-grained variable, analogous to extending Brownian motion to a planar geometry. In fact, the same expression for the friction as Eq. (24) would result had we chosen to work in the liquid's frame of reference and written the Langevin equation as

$$M_w\frac{dU(t)}{dt} = -\lambda_{\text{eff}}\mathcal{A}U(t) + F^R(t), \tag{26}$$

where M_w and U are the mass and velocity of the solid wall, respectively. When the flow profile is plug-like, $U \to -\bar{v}_x \approx -v_s$ and, as discussed above, $\lambda_{\text{eff}} \approx \lambda_{\text{intr}}$. In this limit, we recover the Langevin equation as written by BB in Ref. 26.

To understand why the transport coefficient defined by the GK relation in Eq. (24) measures an effective friction coefficient, not the intrinsic friction coefficient λ_{intr} that enters Navier's constitutive relation Eq. (2), it is again helpful to draw analogy to Brownian motion: a spherical particle moving with a constant velocity $\boldsymbol{v}$ in the solvent will have a total frictional force $\boldsymbol{F} = -\xi\boldsymbol{v}$, where the friction coefficient ξ in this case depends on the slippage boundary condition at the sphere's surface, the sphere's radius, and the solvent's viscosity. While this is simply a statement of Stokes' law, it gives an example of a constitutive relation relating the total friction to the velocity of the moving object, not the slip velocity at the boundary like in Navier's constitutive relation.

A constitutive relation associated with λ_{eff} can be obtained using linear response theory. To this end, we imagine moving the liquid droplet at a steady-state velocity of $\bar{v}_x$ relative to the surface. The perturbed Hamiltonian is

$$\mathcal{H}_c' = \mathcal{H}_c + \bar{v}_x\hat{\boldsymbol{e}}_x \cdot \sum_{i=1}^{N}\boldsymbol{p}_i, \tag{27}$$

where $\mathcal{H}_c$ is the unperturbed Hamiltonian and $\bar{v}_x\hat{\boldsymbol{e}}_x$ plays the role of the external field that couples to the liquid momentum as the conjugate variable. To make a connection with λ_{eff} in Eq. (24), we consider

the response of F_x under constrained dynamics. In this case, the momentum conservation constraint would maintain the liquid's linear momentum at zero ($P_x = 0$) at equilibrium and at $P_x = M\bar{v}_x$ out-of-equilibrium. Using linear response theory[59] (detailed in the supplementary material), we show that the response of the tangential frictional force to a small but finite perturbation $\bar{v}_x\hat{\boldsymbol{e}}_x$ is

$$\langle F_x\rangle_c' = -\beta\int_0^\infty \mathrm{d}t\ \langle F_x(t)F_x(0)\rangle_c\bar{v}_x, \tag{28}$$

where $\langle\ldots\rangle_c'$ and $\langle\ldots\rangle_c$ denote a constrained ensemble average out-of-equilibrium and at equilibrium, respectively. By combining Eq. (28) with the GK relation in Eq. (24), we arrive at a constitutive relation between the frictional force and the steady-state velocity of the liquid,

$$F_x = -\lambda_{\mathrm{eff}}\mathcal{A}\bar{v}_x. \tag{29}$$

Here, we have dropped the canonical average on the force when writing the constitutive relation. This expression is in fact analogous to Stoke's law, and λ_{eff} therefore depends not only on the slippage boundary conditions and the viscosity of the liquid but also on the size and shape of the liquid.

Applying the framework that we have derived to confined fluids is straightforward; the total frictional force on the liquid (F_x) now contains contributions from all solid surfaces in contact with the fluid, while v_x is simply the average flow velocity of the fluid. To verify Eq. (29), we considered systems with water confined in four symmetric channels made up of solid substrates with attractive strengths of $\varepsilon_{\mathrm{wf}} = \alpha\varepsilon_0$, where the "wetting coefficients" are $\alpha = 1, 2, 3, 4$ and $\varepsilon_0 = 1.57$ kJ mol^{-1}. We also consider one asymmetric channel with $\alpha = 1$ for the top wall and $\alpha = 4$ for the bottom wall. Various channel heights between the first atomic planes of the solids are considered, $H/\mathrm{nm} \approx 1.4, 2.7, 5.2$. Details on the systems and molecular models can be found in the supplementary material. Using constrained EMD simulations, we computed λ_{eff} from the GK relation in Eq. (24). For reference NEMD simulations, we performed simulations of Poiseuille flow by applying a body force on each oxygen atom to mimic the effect of a pressure gradient. In the regime of low driving force, the linear response predicted by λ_{eff} obtained from constrained EMD simulations (labeled GK*) is in excellent agreement with $\bar{v}_x$ measured from NEMD simulations, shown for channels of different attractive strengths in Fig. 2(a) and for channels of different heights in the supplementary material. In the supplementary material (Fig. S3), we also confirmed the equivalence between the equilibrium and out-of-equilibrium force autocorrelation, as expected from the fluctuation–dissipation theorem in the linear response regime.

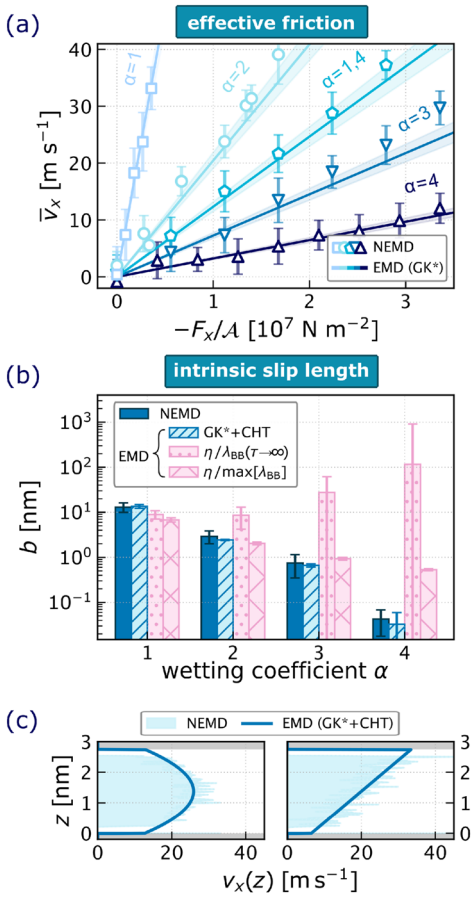

FIG. 2. Connection between microscopic friction and macroscopic hydrodynamics. (a) Verification of the constitutive relation in Eq. (29) between the total frictional force and the mean fluid velocity for the effective friction. The data points are from NEMD simulations of Poiseuille flow in 2D channels of water confined with surfaces of different wetting coefficients α. The solid lines have slopes $1/\lambda_{\mathrm{eff}}$, where λ_{eff} has been obtained from the GK relation with constrained EMD simulations [Eq. (32), label GK*]. (b) The slip lengths obtained from Eq. (31), using λ_{eff} from EMD simulations [Eq. (32)], labeled GK*+CHT, are in excellent agreement with those using λ_{eff} from linear fits to NEMD data points in (a). Meanwhile, the performance of the BB formula, either by taking the long time limit $\lambda_{\mathrm{BB}}(\tau\to\infty)$ or by taking the maximum value $\max[\lambda_{\mathrm{BB}}]$, and interpreting it as an intrinsic friction coefficient [Eq. (3)], gets worse as the surface becomes more attractive. (c) Very good agreement is also obtained for the predicted velocity profile using our approach (GK* + CHT) and reference NEMD data, shown for the case $\alpha = 3$ for both Poiseuille (left) and Couette (right) flows.

B. Connection to the hydrodynamic slip boundary

While the GK relation provides a microscopic expression for the effective friction, more often than not, one is interested in the intrinsic friction or the slip length of a particular interface. Since the constitutive relation of the effective friction has been established, it is relatively straightforward to obtain a relationship between the effective friction and the slip length from macroscopic hydrodynamics. In particular, we can solve the Navier–Stokes equation[60,61] subject to partial slip boundary conditions like Eq. (1) at the solid wall to obtain the Poiseuille flow profile of the fluid. From the solution, we then obtain the fluid velocity and its frictional force per unit area, the ratio of which gives an expression for the effective friction coefficient. Here, we will simply state the results for the common cases of 2D and 1D confinement, with the details presented in the supplementary material.

For 2D confinement, the CHT result for the effective friction of a fluid of shear viscosity η confined in a channel of height H, made up of two separate interfaces, is

$$\lambda_{\text{eff}}^{\text{2D}}(H) = \frac{12(H + b_1 + b_2)\eta}{H^2 + 4H(b_1 + b_2) + 12b_1b_2}, \tag{30}$$

where b_1 and b_2 are the slip lengths of each interface. To obtain a closed expression for the slip length of a single interface, we can consider the case when the channel is symmetric, i.e., $b_1 = b_2 = b$, and rearrange Eq. (30),

$$b = \left(\frac{\eta}{\lambda_{\text{eff}}^{\text{2D}}(H)} - \frac{H}{3}\right) + \left[\left(\frac{\eta}{\lambda_{\text{eff}}^{\text{2D}}(H)} - \frac{H}{3}\right)^2 + H\left(\frac{\eta}{\lambda_{\text{eff}}^{\text{2D}}(H)} - \frac{H}{12}\right)\right]^{1/2}. \tag{31}$$

The effective friction in a 2D channel can be computed with the GK expression,

$$\lambda_{\text{eff}}^{\text{2D}} = \frac{\beta}{2\mathcal{A}}\int_0^\infty \mathrm{d}t\, \langle \boldsymbol{F}_\parallel(t)\cdot\boldsymbol{F}_\parallel(0)\rangle_{\text{c}}, \tag{32}$$

from an EMD simulation with a constraint keeping the liquid's linear momentum zero in the in-plane (x, y) directions, where $\boldsymbol{F}_\parallel = (F_x, F_y)$ denotes the in-plane lateral force on the liquid.

For 1D confinement, we consider Poiseuille flow of a fluid through a cylindrical tube of radius R. In an analogous manner, the effective friction coefficient can be obtained from classical hydrodynamics as

$$\lambda_{\text{eff}}^{\text{1D}}(R) = \frac{4\eta}{R + 4b_R}, \tag{33}$$

where the slip length b_R is in general dependent on the curvature and therefore the radius of the tube. Rearranging for b_R, we obtain

$$b_R = \frac{\eta}{\lambda_{\text{eff}}^{\text{1D}}(R)} - \frac{R}{4}, \tag{34}$$

where $\lambda_{\text{eff}}^{\text{1D}}$ can be obtained with

$$\lambda_{\text{eff}}^{\text{1D}} = \frac{\beta}{\mathcal{A}}\int_0^\infty \mathrm{d}t\, \langle F_z(t)F_z(0)\rangle_{\text{c}}, \tag{35}$$

from an EMD simulation with a constraint keeping the liquid's momentum zero along the axial direction (z) of the tube, where F_z denotes the force on the liquid in the axial direction.

The pair of Eqs. (31)/(32) and (34)/(35) provides a way to obtain hydrodynamic slippage directly from fluctuating forces in microscopic EMD simulations. In Fig. 2(b), we validate that the slip lengths b obtained by this method (labeled GK* + CHT) are in excellent agreement with results from reference NEMD simulations for surfaces of different values of wettability. (To obtain b from NEMD, we have measured λ_{eff} and used the result in the CHT expression, rather than attempt to fit the flow profiles directly.) In contrast, using the BB expression in Eq. (4) combined with Eq. (3), as is typically done in the literature, significantly overpredicts the slip length as the wettability increases.

While sources of uncertainty in the effective friction measured with the GK relation arise from statistical error, the value of slip length is also impacted by the choice of hydrodynamic boundary position z_0 [which enters Eqs. (31) and (34) implicitly through H and R]. While approaches exist for determining z_0, see, e.g., Refs. 62 and 63, here we make the pragmatic choice to place z_0 at the first plane of solid atoms in contact with the liquid. With this choice, the solution for the velocity profile from the Navier–Stokes equation spans the total height of the channel or the diameter of the cylindrical tube. However, microscopically, there is potentially an offset in the location of the hydrodynamic boundary due to the excluded volume at each liquid–solid interface. In the supplementary material, we assess the sensitivity of our results to such an offset. We find that, when the fluid's friction is dominated by viscous dissipation (i.e., in tubes or channels that are large compared to the slip length), results are robust to reasonable choices of z_0. As H or R tends to zero, the obtained values of b become increasingly sensitive to the choice of z_0; generally speaking, in cases where $H > 1$ nm, placing the hydrodynamic boundary at the first atomic plane of the solid is a reasonable approximation.

It is important to note that the appropriate type of flow used to give the mapping between CHT and the effective friction is Poiseuille flow, where the fluid has been driven by a pressure gradient or a body force. This is because under confinement, when the liquid is in contact with two separate solid substrates, the solid's frame of reference is only well-defined when both substrates have the same velocity as each other. Note that the mapping to Poiseuille flow enables calculation of friction in cylindrical geometries. Meanwhile, in the case of Couette flow, the two solid substrates are moving at different velocities in order to shear the fluid. However, as the slip length b is an intrinsic property, once its value is known, predictions of the velocity profile can be obtained from CHT. For example, we show the predictions for the symmetric $\alpha = 3$ channel, both for Couette flow and for Poiseuille flow in Fig. 2(c), and for other cases extensively in the supplementary material. In all cases, we find very good agreement with reference NEMD simulations.

IV. APPLICATION: WATER FRICTION UNDER CONFINEMENT

Having a connection between a macroscopic and microscopic description of fluid flow, we can revisit the long-standing question on the domain of applicability of the continuum hydrodynamic equations. Such a question is twofold, as it concerns both the validity of the boundary conditions applied when solving the Navier–Stokes equation and the validity of continuum hydrodynamics itself.

Historically, the no-slip boundary condition $b = 0$ can successfully describe much of everyday phenomena involving fluid dynamics.[64,65] For water flowing through macroscopic tubes and channels, it provides a very good approximation, regardless of the material of the solid wall. At these larger scales, the effective friction increases monotonically as the tube becomes smaller, $\lambda_{\text{eff}}^{\text{1D}} \sim 4\eta/R$, or as the channel height decreases, $\lambda_{\text{eff}}^{\text{2D}} \sim 12\eta/H$. It has also long been established that as the length scale of confinement keeps shrinking in size, finite slippage at the interface can no longer be ignored[66,67] as a larger proportion of the confined fluid can feel the interface. Thus, the first question we will address is as follows: "*At which confinement length scale do surface effects begin to manifest as a deviation from the no-slip boundary approximation?*" The answer will depend on various factors, including the material and the curvature of confinement.

To answer this question, we will consider 1D confinement in single-walled carbon and boron nitride nanotubes of different radii and 2D confinement in channels of different heights formed by two

graphene or boron nitride sheets. For the interatomic interaction, we employ a machine-learned potential where the electronic structure is accurately trained at the level of density functional theory;[17] the walls are flexible in these simulations. While we consider these low-dimensional materials for their relevance to applications in nanofluidics, we stress the generality of the results obtained to confinement by other solid surfaces of other liquids. While the microscopic mechanisms giving rise to friction at the interface are very diverse (corrugation,[14,17] phonon coupling,[13] quantum friction,[20,68] defects,[42,46,47] etc.) and we expect them to depend sensitively on the molecular details of the interface, the macroscopic hydrodynamic behavior would be principally governed by the slip length. Therefore, in addition to these realistic surfaces, we also consider water confined in Lennard-Jones nanotubes and between walls of different values of wettability.

For each surface, we first obtain the slip length from EMD simulations using the pair of Eqs. (31)/(32) and (34)/(35). Among the different wall materials, the graphene surface has the highest slip length (b = 16 nm), followed by boron nitride (b = 3.6 nm) and the Lennard-Jones surface of high wettability where there is essentially no slippage. In the case of 1D confinement, in addition to surface effects due to different confining materials, curvature effects also come into play since curving up a surface can change its free energy surface significantly. We show the curvature-dependent slip length b_R for three different surfaces in Fig. 3(a). In all cases, curving up the surface to form nanotubes leads to a decrease in the corrugation of the surface, reflected by an increase in b_R as R decreases. This enhancement is most prominent for tubes of $R \lesssim 5$ nm with the slippery carbon surface. Our values are broadly in agreement with previous simulations and experiments of water on graphene and boron nitride surfaces.[10,12,14,16,17,20]

To assess the overall effect of changing the radius on water flow in 1D confinement, using $b_R(R)$ obtained from a non-linear fit of the simulation data in [Eq. (30)], we show in Fig. 3(b) the effective friction $\lambda_{\text{eff}}^{\text{1D}}$ as a function of R. There are two competing effects dictating the behavior of $\lambda_{\text{eff}}^{\text{1D}}$. For tubes with diameters on the micrometer scale and beyond, $\lambda_{\text{eff}}^{\text{1D}}$ increases as R decreases for all surfaces, asymptotic to the no-slip prediction. As R reaches the nanometric regime, since it is now comparable to b_R, the effective friction in the fluid is no longer agnostic to the amount of slippage taking place at the wall. As a result, the enhancement in b_R due to curvature effects starts to dominate, decreasing $\lambda_{\text{eff}}^{\text{1D}}$ as R decreases. Therefore, a crossover in the dependence of $\lambda_{\text{eff}}^{\text{1D}}$ on R can be observed at $R \sim 10$ nm and is most significant for surfaces of the highest slippage. We note that experiments[10] with multi-walled carbon nanotubes have reported a radius dependence of slip length up to 50 nm, so the length scale of the crossover could be as large as tens of nanometers. For 2D confinement, since there is no curvature effect, any surface effect would be solely due to interactions between the solid and the fluid. In this case, instead of a crossover, a deviation to the no-slip prediction is seen for the asymptotic behavior of $\lambda_{\text{eff}}^{\text{2D}}$ as the channel height H decreases, as shown in Fig. 3(c) for water confined in symmetric channels of graphene, hexagonal boron nitride, and the Lennard-Jones solid substrates. Similarly, the length scale of this deviation is in the tens of nanometers and is most significant for surfaces of the highest slippage.

Hydrodynamics relies on the key assumption that the fluid behaves as a continuum in the hydrodynamic regime, where the local properties of the fluid vary slowly on microscopic time and length scales.[52] As the degree of confinement increases, this approximation is expected to break down as the separation in scale between the confinement length and the molecular length becomes less clear. This naturally brings us to the second question: "*Once finite slippage is accounted for at the interface, what is the confinement length scale at which it is still possible to describe flow with continuum hydrodynamics?*"

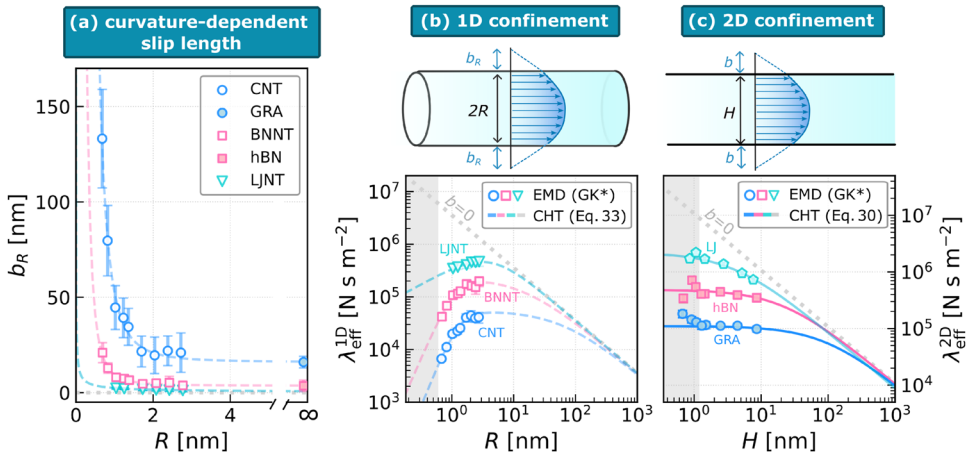

FIG. 3. Water friction under confinement. (a) Curvature dependence of the slip length b for water on different surfaces, including carbon nanotubes (CNTs), boron nitride nanotubes (BNNTs), nanotubes made of Lennard-Jones particles (LJNTs), a flat graphene sheet (GRA), and a flat hexagonal boron nitride sheet (hBN), obtained from simulations. The effective friction under 1D and 2D confinement is shown in (b) and (c) as a function of the tube radius R and channel height H. The data points are obtained by the GK relation using constrained EMD simulations. For 2D confinement, the solid lines are predictions from CHT [Eq. (30)] parameterized on the slip length of the largest channel. For 1D confinement, the dashed lines are from Eq. (33) using $b_R(R)$ fitted to the simulation data. The dotted lines show the results using no-slip boundary conditions, while solid lines account for finite slippage at the interface. The shaded regions indicate where CHT begins to break down.

Since the GK relation we have derived is independent of CHT, we can parameterize CHT with the slip length obtained from a particular geometry and then assess how well this parameterized CHT performs as we decrease the confinement length. To this end, we compare the effective friction predicted by CHT [Eq. (30)] with that computed from the GK relation for various channel heights down to the sub-nanometer regime, shown as data points in Fig. 3(c). We find that in all confining materials considered, CHT predictions hold remarkably well down to $H \sim 1$ nm, where the channels can accommodate only three layers of water. The deviation between CHT and simulations is only significant for smaller channels with a bilayer and monolayer of water, where we find that $\lambda_{\text{eff}}^{\text{2D}}$ from simulations is extremely sensitive to changes in the density and interfacial structure of the fluid. The breakdown of CHT below 1 nm is perhaps not surprising since with fewer than three layers of water, one can no longer sensibly define a continuum bulk region. In fact, the length scale of 1 nm has been suggested both experimentally[69,70] and theoretically[71,72] as the limit for the validity of the notion of a bulk shear viscosity. Nevertheless, the robustness of a continuum theory to describe water flow down to such a small scale is extremely satisfying. It is also reminiscent of the validity of other macroscopic theories, e.g., continuum mechanics,[73] the Kelvin equation,[74] or dielectric continuum theory,[75–78] down to the nanoscale.

V. CONCLUSION

In this work, through the use of the projection operator formalism and linear response theory, we have derived a GK relation for the liquid–solid friction by considering the stochastic motion of a liquid droplet on a solid surface. The force autocorrelation function in the expression is sampled using constrained dynamics in which the momentum of the liquid is conserved. Not only does such an expression help resolve the long-standing plateau problem associated with previous studies of friction using molecular simulations, but it also sheds light on the physical meaning of the obtained friction coefficient: λ_{eff} measures an effective friction and not the intrinsic interfacial friction. Our expression can be applied generally to finite systems with surfaces of very low or very high friction. In contrast, the widely used expression by Bocquet and Barrat was derived originally for a semi-infinite system.[26,30] When applied to finite systems, in the context of our work, it amounts to a reasonable approximation only when the slip length is much greater than the confining length scale.

By linking the microscopic expression for friction to macroscopic hydrodynamics, we show how the hydrodynamic slip length can be obtained faithfully, for both 1D and 2D fluid flow. Going forward, we believe that such a connection is important to understand the flow of liquids across length scales on more complex surfaces where slippage is determined by the interplay of the material's electronic properties, wettability, surface charge, and the presence of defects. This work also lays the foundation for understanding interfacial effects in electrokinetic phenomena and other transport properties under confinement.[79,80] We believe that our work can provide insights for the development of microscopic descriptions of hydrodynamics based on dynamical density functional theory[63,81–83] and the non-equilibrium extension of equilibrium classical density functional theory,[52,84,85] in which the fluid flow is described with mass and momentum density fields.

Finally, as an application of our approach, we assess the ability of continuum hydrodynamics to describe water flow at the nanoscale. While for macroscopic confining geometries, assuming no-slip boundary conditions is a reasonable approximation, the impact of finite slippage cannot be ignored for confinement length scales below 10–100 nm. Nevertheless, our results show that, provided that the finite slip length is taken into account, continuum hydrodynamics remains remarkably robust down to ~1 nm confinement.

SUPPLEMENTARY MATERIAL

The supplementary material includes simulations details and additional supporting results.

ACKNOWLEDGMENTS

We thank Mathieu Salanne, Laurent Joly, and Daan Frenkel for insightful discussions. Via membership of the UK's HEC Materials Chemistry Consortium funded by EPSRC (No. EP/X035859), this work used the ARCHER2 UK National Supercomputing Service. A.T.B. acknowledges funding from the Oppenheimer Fund and Peterhouse College, University of Cambridge. S.J.C. is a Royal Society University Research Fellow (Grant No. URF\R1\211144).

AUTHOR DECLARATIONS

Conflict of Interest

The authors have no conflicts to disclose.

Author Contributions

Anna T. Bui: Conceptualization (equal); Investigation (equal); Writing – original draft (equal); Writing – review & editing (equal). **Stephen J. Cox**: Conceptualization (equal); Investigation (equal); Writing – original draft (equal); Writing – review & editing (equal).

DATA AVAILABILITY

The data that support the findings of this study are openly available at the University of Cambridge Data Repository at https://doi.org/10.17863/CAM.111725. Scripts for computing the friction coefficient are available at https://github.com/annatbui/friction-GK.

REFERENCES

[1] A. Siria, P. Poncharal, A.-L. Biance, R. Fulcrand, X. Blase, S. T. Purcell, and L. Bocquet, Nature **494**, 455 (2013).
[2] L. Joly, R. H. Meißner, M. Iannuzzi, and G. Tocci, ACS Nano **15**, 15249 (2021).
[3] L. Bocquet, Nat. Mater. **19**, 254 (2020).
[4] A. K. Geim and I. V. Grigorieva, Nature **499**, 419 (2013).
[5] K. Celebi, J. Buchheim, R. M. Wyss, A. Droudian, P. Gasser, I. Shorubalko, J.-I. Kye, C. Lee, and H. G. Park, Science **344**, 289 (2014).
[6] A. Bhardwaj, M. V. Surmani Martins, Y. You, R. Sajja, M. Rimmer, S. Goutham, R. Qi, S. Abbas Dar, B. Radha, and A. Keerthi, Nat. Protoc. **19**, 240 (2024).

[7]J. K. Holt, H. G. Park, Y. Wang, M. Stadermann, A. B. Artyukhin, C. P. Grigoropoulos, A. Noy, and O. Bakajin, Science **312**, 1034 (2006).
[8]M. Majumder, N. Chopra, R. Andrews, and B. J. Hinds, Nature **438**, 44 (2005).
[9]M. Whitby, L. Cagnon, M. Thanou, and N. Quirke, Nano Lett. **8**, 2632 (2008).
[10]E. Secchi, S. Marbach, A. Niguès, D. Stein, A. Siria, and L. Bocquet, Nature **537**, 210 (2016).
[11]R. H. Tunuguntla, R. Y. Henley, Y.-C. Yao, T. A. Pham, M. Wanunu, and A. Noy, Science **357**, 792 (2017).
[12]A. Keerthi, S. Goutham, Y. You, P. Iamprasertkun, R. A. W. Dryfe, A. K. Geim, and B. Radha, Nat. Commun. **12**, 3092 (2021).
[13]M. Ma, G. Tocci, A. Michaelides, and G. Aeppli, Nat. Mater. **15**, 66 (2016).
[14]K. Falk, F. Sedlmeier, L. Joly, R. R. Netz, and L. Bocquet, Nano Lett. **10**, 4067 (2010).
[15]J. A. Thomas and A. J. H. McGaughey, Nano Lett. **8**, 2788 (2008).
[16]G. Tocci, L. Joly, and A. Michaelides, Nano Lett. **14**, 6872 (2014).
[17]F. L. Thiemann, C. Schran, P. Rowe, E. A. Müller, and A. Michaelides, ACS Nano **16**, 10775 (2022).
[18]G. Hummer, J. C. Rasaiah, and J. P. Noworyta, Nature **414**, 188 (2001).
[19]A. Kalra, S. Garde, and G. Hummer, Proc. Natl. Acad. Sci. U. S. A. **100**, 10175 (2003).
[20]A. T. Bui, F. L. Thiemann, A. Michaelides, and S. J. Cox, Nano Lett. **23**, 580 (2023).
[21]A. Striolo, Nano Lett. **6**, 633 (2006).
[22]C.-L. Navier, Mem. Acad. Sci. Inst. France **6**, 389 (1823).
[23]M. Cieplak, J. Koplik, and J. R. Banavar, Phys. Rev. Lett. **86**, 803 (2001).
[24]S. K. Kannam, B. D. Todd, J. S. Hansen, and P. J. Daivis, J. Chem. Phys. **136**, 024705 (2012).
[25]L. Bocquet and J.-L. Barrat, Phys. Rev. E **49**, 3079 (1994).
[26]L. Bocquet and J.-L. Barrat, J. Chem. Phys. **139**, 044704 (2013).
[27]J. G. Kirkwood, J. Chem. Phys. **14**, 180 (1946).
[28]P. Mazur and I. Oppenheim, Physica **50**, 241 (1970).
[29]P. Español and I. Zúñiga, J. Chem. Phys. **98**, 574 (1993).
[30]L. Bocquet, J.-P. Hansen, J. Piasecki, and J. Stat, J. Stat. Phys. **89**, 321 (1997).
[31]R. Kubo, M. Toda, and N. Hashitsume, *Statistical Physics II: Nonequilibrium Statistical Mechanics* (Springer Berlin Heidelberg, 2012).
[32]J. A. de la Torre, D. Duque-Zumajo, D. Camargo, and P. Español, Phys. Rev. Lett. **123**, 264501 (2019).
[33]H. Oga, Y. Yamaguchi, T. Omori, S. Merabia, and L. Joly, J. Chem. Phys. **151**, 054502 (2019).
[34]H. Oga, T. Omori, L. Joly, and Y. Yamaguchi, J. Chem. Phys. **159**, 024701 (2023).
[35]S. Chen, H. Wang, T. Qian, and P. Sheng, Phys. Rev. E **92**, 043007 (2015).
[36]J. Petravic and P. Harrowell, J. Chem. Phys. **127**, 174706 (2007).
[37]J. S. Hansen, B. D. Todd, and P. J. Daivis, Phys. Rev. E **84**, 016313 (2011).
[38]K. Huang and I. Szlufarska, Phys. Rev. E **89**, 032119 (2014).
[39]B. Ramos-Alvarado, S. Kumar, and G. P. Peterson, Phys. Rev. E **93**, 023101 (2016).
[40]H. Nakano and S.-i. Sasa, Phys. Rev. E **101**, 033109 (2020).
[41]S. Varghese, J. S. Hansen, and B. D. Todd, J. Chem. Phys. **154**, 184707 (2021).
[42]H. Li, W. Guo, and Y. Guo, J. Phys. Chem. Lett. **15**, 6585 (2024).
[43]C. Liang and N. R. Aluru, ACS Nano **18**, 16141 (2024).
[44]G. Tocci, M. Bilichenko, L. Joly, and M. Iannuzzi, Nanoscale **12**, 10994 (2020).
[45]A. Kumar Verma and A. Govind Rajan, Langmuir **38**, 9210 (2022).
[46]A. Seal and A. Govind Rajan, Nano Lett. **21**, 8008 (2021).
[47]L. Joly, G. Tocci, S. Merabia, and A. Michaelides, J. Phys. Chem. Lett. **7**, 1381 (2016).
[48]R. Zwanzig, Phys. Rev. **124**, 983 (1961).
[49]H. Mori, Prog. Theor. Phys. **33**, 423 (1965).
[50]R. Zwanzig, *Nonequilibrium Statistical Mechanics*, 3rd ed. (Oxford University Press, 2001).
[51]B. Berne and R. Pecora, *Dynamic Light Scattering: With Applications to Chemistry, Biology, and Physics* (Dover Publications, 2000).
[52]J. Hansen and I. McDonald, *Theory of Simple Liquids: With Applications to Soft Matter*, 4th ed. (Elsevier Science, 2013).
[53]C. Hijón, P. Español, E. Vanden-Eijnden, and R. Delgado-Buscalioni, Faraday Discuss. **144**, 301 (2010).
[54]P. Español, J. A. de la Torre, and D. Duque-Zumajo, Phys. Rev. E **99**, 022126 (2019).
[55]A. Carof, R. Vuilleumier, and B. Rotenberg, J. Chem. Phys. **140**, 124103 (2014).
[56]C. Ayaz, L. Scalfi, B. A. Dalton, and R. R. Netz, Phys. Rev. E **105**, 054138 (2022).
[57]A. J. Dominic, T. Sayer, S. Cao, T. E. Markland, X. Huang, and A. Montoya-Castillo, Proc. Natl. Acad. Sci. U. S. A. **120**, e2221048120 (2023).
[58]J.-L. Barrat and L. Bocquet, Faraday Discuss. **112**, 119 (1999).
[59]D. J. Evans and G. Morriss, *Statistical Mechanics of Nonequilibrium Liquids*, 2nd ed. (Cambridge University Press, 2008).
[60]L. Landau and E. Lifshitz, *Statistical Physics* (Elsevier Science, 2013), Vol. 5.
[61]R. Bird, W. Stewart, and E. Lightfoot, *Transport Phenomena* (J. Wiley, 2002).
[62]C. Herrero, T. Omori, Y. Yamaguchi, and L. Joly, J. Chem. Phys. **151**, 041103 (2019).
[63]D. Camargo, J. A. de la Torre, R. Delgado-Buscalioni, F. Chejne, and P. Español, J. Chem. Phys. **150**, 144104 (2019).
[64]R. Feynman, R. Leighton, and M. Sands, *The Feynman Lectures on Physics* (Addison-Wesley Publishing Company, 1963), Vol. III.
[65]S. Goldstein, *Modern Developments in Fluid Dynamics* (Clarendon Press, 1950), Vol. I.
[66]Y. Zhu and S. Granick, Phys. Rev. Lett. **88**, 106102 (2002).
[67]P. A. Thompson and S. M. Troian, Nature **389**, 360 (1997).
[68]N. Kavokine, M.-L. Bocquet, and L. Bocquet, Nature **602**, 84 (2022).
[69]U. Raviv and J. Klein, Science **297**, 1540 (2002).
[70]T.-D. Li, J. Gao, R. Szoszkiewicz, U. Landman, and E. Riedo, Phys. Rev. B **75**, 115415 (2007).
[71]Y. Leng and P. T. Cummings, Phys. Rev. Lett. **94**, 026101 (2005).
[72]L. Bocquet and E. Charlaix, Chem. Soc. Rev. **39**, 1073 (2010).
[73]Y. Mo, K. T. Turner, and I. Szlufarska, Nature **457**, 1116 (2009).
[74]Q. Yang, P. Z. Sun, L. Fumagalli, Y. V. Stebunov, S. J. Haigh, Z. W. Zhou, I. V. Grigorieva, F. C. Wang, and A. K. Geim, Nature **588**, 250 (2020).
[75]S. J. Cox and P. L. Geissler, Chem. Sci. **13**, 9102 (2022).
[76]P. Loche, C. Ayaz, A. Wolde-Kidan, A. Schlaich, and R. R. Netz, J. Phys. Chem. B **124**, 4365 (2020).
[77]S. J. Cox and P. L. Geissler, J. Chem. Phys. **148**, 222823 (2018).
[78]A. Schlaich, E. W. Knapp, and R. R. Netz, Phys. Rev. Lett. **117**, 048001 (2016).
[79]L. Joly, C. Ybert, E. Trizac, and L. Bocquet, J. Chem. Phys. **125**, 204716 (2006).
[80]P. Simonnin, B. Noetinger, C. Nieto-Draghi, V. Marry, and B. Rotenberg, J. Chem. Theory Comput. **13**, 2881 (2017).
[81]D. Camargo, J. A. de la Torre, D. Duque-Zumajo, P. Español, R. Delgado-Buscalioni, and F. Chejne, J. Chem. Phys. **148**, 064107 (2018).
[82]U. M. B. Marconi and P. Tarazona, J. Phys.: Condens. Matter **12**, A413 (2000).
[83]P. Español and H. Löwen, J. Chem. Phys. **131**, 244101 (2009).
[84]R. Evans, Adv. Phys. **28**, 143 (1979).
[85]A. T. Bui and S. J. Cox, J. Chem. Phys. **161**, 104103 (2024).